



# Corrosion resistance of functionalized carbon nanotubes enhanced epoxy coatings on sintered NdFeB magnets

Hongyi Yang, Liangsong Duan, Pengjie Zhang, Guangqing Xu , Jiewu Cui, Jun Lv, Wei Sun, Bingshan Li, Dongmei Wang, Yucheng Wu

Received: 13 December 2021 / Revised: 10 March 2022 / Accepted: 13 March 2022  
© American Coatings Association 2022

**Abstract** In this work, tannic acid (TA) was employed to modify the surface of multiwall carbon nanotubes (CNTs) to form TCNTs hybrids via noncovalent functionalization to enhance its dispersibility in water. Then, the TCNTs enhanced epoxy coatings were applied on sintered NdFeB magnets by cathodic electrophoretic deposition method for corrosion test. The corrosion resistance of prepared specimens was assessed by electrochemical experiments. The results show that TCNTs hybrids present a more homogeneous distribution in epoxy resin than pristine CNTs and could obviously promote anticorrosion properties of prepared specimens. Within 36-day soaking in 3.5 wt.% NaCl solution, the specimens maintain a high value of  $|Z|_{0.01\text{Hz}}$  ( $10^8 \Omega \text{cm}^2$ ) when the concentration

of TCNTs is 2 g/L. When immersed in 3.5 wt.% NaCl solution for 40 days, the  $E_{\text{corr}}$  of specimens shifts to  $-0.207 \text{ V}$  and  $J_{\text{corr}}$  is about  $5.281 \times 10^{-11} \text{ A cm}^{-2}$ , which demonstrates superior corrosion resistance.

**Keywords** NdFeB magnets, Carbon nanotubes, Tannic acid functionalization, Epoxy coatings, Corrosion resistance

## Introduction

Since sintered NdFeB magnets were firstly reported in 1980, they have been diffusely used in various industrial sectors, such as electroacoustic, electronic, and motor, due to their outstanding magnetic properties.<sup>1–3</sup> However, the absence of corrosion resistance in corrosive environment limits their further application and development in numerous fields, which is mainly related to the characteristics of preparation process and material structure of magnets. For one thing, NdFeB magnets fabricated by sintering process have many defects such as sintering pores and low density.<sup>4</sup> For the other, NdFeB magnets have a multiphase structure, consisting of the matrix phase  $\text{Nd}_2\text{Fe}_{14}\text{B}$ , B-rich, and Nd-rich phase.<sup>5</sup> The electrochemical potential of each phase varies greatly, which is prone to electrochemical corrosion.

Currently, the routes for alleviating the corrosion of NdFeB magnets mainly utilize alloying and surface coatings. The alloying technology mainly optimizes the magnetic structure and reduces the potential difference of each phase by adding alloy elements represented by Dy, Ce, Cu, Al, Co, and Ti,<sup>6–10</sup> so as to promote the corrosion resistance of the magnet itself. However, it will also reduce the magnetic properties and increase the production cost of magnets. Therefore, surface coatings are a more effective way to alleviate the corrosion of magnets; that is, the coating is used to

This paper was presented at the Surfaces, Interfaces and Coatings Technology International Conference that was held virtually from April 7–9, 2021.

H. Yang, L. Duan, G. Xu (✉), J. Cui, J. Lv,  
D. Wang, Y. Wu (✉)  
School of Materials Science and Engineering, Hefei  
University of Technology, Hefei 230009, China  
e-mail: gqxu1979@hfut.edu.cn

Y. Wu  
e-mail: yewu@hfut.edu.cn

P. Zhang, W. Sun, B. Li  
BGRIMM Technology Group Co, Ltd, Beijing 102600,  
China

P. Zhang, W. Sun, B. Li  
National Engineering Research Center for Magnetic  
Materials, Beijing 102600, China

G. Xu, J. Cui, J. Lv, D. Wang, Y. Wu  
Key Laboratory of Advanced Functional Materials and  
Devices of Anhui Province, Anhui Provincial International  
S&T Cooperation Base for Advanced Energy Materials,  
Hefei University of Technology, Hefei 230009, China

establish a barrier film between the magnets and the corrosive environment, so as to prevent the invasion of external corrosive medium (such as  $\text{H}_2\text{O}$ ,  $\text{O}_2$ , and  $\text{Cl}^-$ ). Among them, epoxy coatings have captured extensive attention for their inexpensiveness, ease of preparation, excellent mechanical properties and adhesion.<sup>11,12</sup> Traditional solvent-base epoxy coatings normally contain a large number of volatile organic compounds, which is harmful to humans and the environment. As a result, environment-friendly waterborne epoxy coatings are gaining increasing attention.<sup>13,14</sup> However, owing to the evaporation of water during solidification process, waterborne epoxy coatings are prone to form micropores defects, resulting in the rapid invasion of external corrosive medium and greatly limiting its industrial application.<sup>15,16</sup> Preparation of composite coatings via addition of diverse nanofillers, such as  $\text{g-C}_3\text{N}_4$ ,  $\alpha\text{-ZrP}$ ,  $\text{Fe}_2\text{O}_3$ , LDHs,  $\text{SiO}_2$ , h-BN,  $\text{Ti}_3\text{C}_2\text{T}_x$ , graphene, and its derivatives, is an efficient way to improve the anticorrosion properties of epoxy coatings by filling the pores inside the coating and increasing tortuosity of invasion paths of aggressive media.<sup>13,15,17–23</sup>

As a kind of one-dimensional nanomaterial with hollow tubular structure, multi-wall carbon nanotubes (CNTs) have many outstanding properties, such as high mechanical and heat stability, large specific surface area, and electrical and chemical inertness, which make it an ideal candidate for organic anticorrosive coatings.<sup>24–27</sup> However, CNTs have poor dispersion in waterborne epoxy coatings owing to their high hydrophobicity as well as high surface energy, which limits their application in waterborne anticorrosion coatings. As a result, a covalent or noncovalent surface modification of CNTs is required to solve this problem. The covalent methods are carried out so as to provide useful functional groups onto the CNTs surface but tend to induce defects on the CNTs sidewalls.<sup>28,29</sup> Compared with covalent modification, noncovalent functionalization is a more appropriate choice due to its less impact on the structure, high efficiency and the convenience of preparation process. For instance, Cui et al.<sup>30</sup> used the  $\pi$ - $\pi$  interaction of poly(2-butylaniline) and CNTs to achieve the efficient dispersion of CNTs in aqueous solution, which further promoted the barrier performance and tribological properties of CNTs/epoxy composite coatings.

In this work, tannic acid (TA), as an eco-friendly plant extract with wide range of sources, was chosen as dispersant to disperse the CNTs for its abundant phenyl and hydroxyl groups. When it mixed with CNTs, the benzene rings of TA could anchor to CNTs' graphite structure via  $\pi$ - $\pi$  interaction so as to lessen their self-aggregation.<sup>31–33</sup> Besides, the hydrophilic hydroxyl groups could be introduced on the surface of CNTs at the same time, which is beneficial to improve the dispersibility of CNTs in water. Then TCNTs hybrids were added into waterborne epoxy coatings to promote the resistance of specimens to corrosion.

## Experiment

### Materials

Commercial sintered NdFeB magnets (unmagnetized 38SH, 12 mm × 13 mm × 3 mm) were provided by Earth-panda Advanced Magnetic Material Co., Ltd. The CNTs with purity of around 95% were supported by Nanjing Xianfeng nanomaterials Co., Ltd. Tannic acid (TA, AR) was provided by Aladdin Chemical Co., Ltd (Shanghai). Nitric acid (AR) and absolute ethyl alcohol (AR) were acquired from Sinopharm Chemical Reagent Co., Ltd. Two components waterborne epoxy resin (EP, HG-90 series, particle size  $\leq 20 \mu\text{m}$ , solid content is  $36 \pm 2\%$ ,  $\text{pH} = 7.0 \pm 0.3$ , conductivity is  $1100 \pm 300 \mu\text{s/cm}$ ) and black slurry (48–52% distilled water, 8–12% 2-butoxyethanol, 5% carbon black, 15% kaolin, 18–22% water-soluble solid) used for coloring were purchased from Brilliant Electrophoresis Co., Ltd (Shenzhen, China). Deionized water with a resistance of  $18.2 \text{ M}\Omega \text{ cm}$  was obtained from a water purification machine.

### Experimental method

#### Preparation of NdFeB substrate

Commercial sintered NdFeB magnets were used as testing substrate in this study. The magnets were immersed in 3 vol.%  $\text{HNO}_3$  for about 40 s, and then sonicated in deionized water to remove surface impurities. Then, they were rinsed with absolute ethyl alcohol, dried with cold air and used for electrodeposition.

#### Preparation of TCNTs hybrids

The synthesis process of TCNTs hybrids is shown in Fig. 1a. First, 200 mg TA was dissolved in 50 mL distilled water with constant agitation to get TA aqueous solution. Then, 50 mg CNTs were added into the TA aqueous solution followed by sonication at 40 KHz for 2 h. The product was collected by vacuum filtration with  $0.1 \mu\text{m}$  polyvinylidene fluoride membrane and then rinsed with deionized water and alcohol three times to eliminate residual TA. Finally, the collected product was vacuum-dried at  $80^\circ\text{C}$  for 10 h to get TCNTs hybrids.

#### Electrodeposition of epoxy coatings

The cathodic electrophoretic deposition process is shown in Fig. 1b. The aqueous EP electrolytes were prepared from the deionized water, waterborne epoxy resin and black slurry at the mass ratio of 4:3:1. Then TCNTs hybrids were introduced into electrolytes with

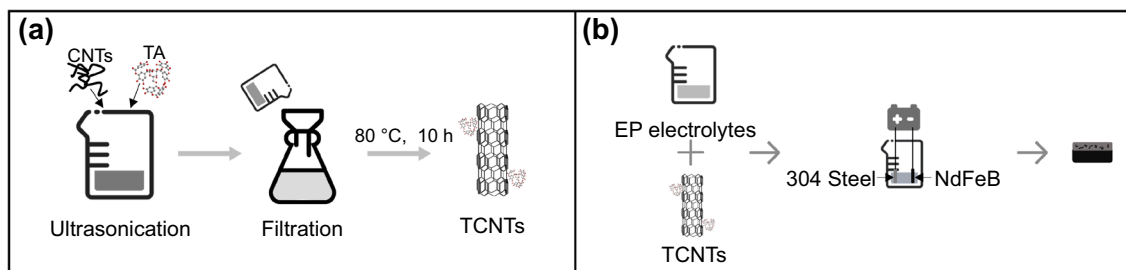


Fig. 1: Schematic illustration of (a) the TCNTs hybrids synthesis procedure and (b) electrodeposition of epoxy coatings

the concentration of 2, 5, and 10 g/L, respectively. Furthermore, pristine CNTs were also introduced into electrolytes with the concentration of 2 g/L for comparison.

A constant voltage method was used for electrodeposition at applied voltage of 60 V for 45 s under stirring condition. The temperature of the electrolytes was maintained at 28°C. The working electrode was sintered NdFeB magnets and counter electrode was 304 stainless steel. After deposition, the specimens were withdrawn from the electrolytes then rinsed with deionized water. Subsequently, all specimens were cured in oven at 90°C for 40 min and 180°C for 30 min. The obtained specimens were named as EP and EP/CNTs<sub>2</sub> for pure epoxy resin specimens and specimens with pristine CNTs added. And for specimens with TCNTs hybrids added, they were named as EP/TCNTs<sub>2</sub>, EP/TCNTs<sub>5</sub>, and EP/TCNTs<sub>10</sub>, respectively.

### Material characterization and corrosion resistance test

Zeta potential of TCNTs hybrids in water was recorded by a Nano ZS90 (Malvern Instruments, UK). X-ray photoelectron spectroscopy (XPS) analysis was completed on an Escalab 250Xi (Thermo, US) with Al K $\alpha$  X-ray source to examine the surface chemical state of TCNTs hybrids. Thermogravimetric analysis (TGA) was recorded on a TGA8000 (PerkinElmer, USA) under an N<sub>2</sub> atmosphere from 20 to 800°C. The crystal structure of TCNTs hybrids was obtained by X-ray diffraction (XRD) on a X-Pert Pro MPD (PANalytical, NL) with Cu K $\alpha$  radiation from 10° to 80° and Raman spectroscopy on a LabRam HR Evolution (HORIBA Jobin Yvon, FR) with  $\lambda = 532$  nm from 800 to 2000 cm<sup>-1</sup>. The morphology of TCNTs hybrids was observed by transmission electron microscopy (TEM) on a JEM-1400 flash (JEOL, JP). The cross section of prepared specimens was observed by field emission scanning electron microscopy (FESEM) on a SU8020 (Hitachi, JP), where the specimens were coated by Au sputtering for 30 s.

The corrosion properties of prepared specimens was assessed by an electrochemical workstation (CHI-660D, Chenhua, Shanghai) in 3.5 wt.% NaCl solution at ambient temperature. A conventional three elec-

trode systems which consisted of a counter electrode (platinum sheet), a working electrode (coated NdFeB magnets with an exposed area of 1 cm<sup>2</sup>) and a reference electrode (saturated calomel electrode) were used in the measurement process. The impedance spectroscopy (EIS) was executed at open circuit potential (OCP) with an AC amplitude of 20 mV over a frequency ranging from 10 mHz to 100 kHz. Potentiodynamic polarization curves were collected from -0.3 to 0.3 V (vs. OCP) at a scan rate of 0.01 V/s. The surface changes of specimens soaked in 3.5 wt.% NaCl solution for a certain time were observed by static immersion corrosion test.

## Results and discussion

### Characterization of TCNTs hybrids

The sedimentation test of CNTs and TCNTs hybrids in water (0.5 mg/mL) is shown in Fig. 2a, which presents the dispersion capacity of CNTs and TCNTs in water. It could be seen that the most of CNTs sink to the bottom of the bottle after 1 h of sonication while TCNTs hybrids present a homogeneous black solution. With increasing storage time to 1 h, CNTs have settled to the bottom of the bottle completely, but there is no obvious precipitation for the TCNTs/water solution after 16 h of storage, indicating that the dispersibility of CNTs in water is significantly improved after the functionalization with TA. The degree of dispersion of CNTs and TCNTs in water is clearly shown in Fig. 2b. It could be observed that CNTs are aggregated severely while there is no similar vison for TCNTs. This is because the lack of hydrophilic groups on the surface of CNTs, coupled with their high specific surface area as well as strong van der Waals forces between the tubes, easily causes aggregation or winding.<sup>34</sup> After the modification of TA, hydrophilic hydroxyl groups were introduced on the surface of CNTs and improved their dispersibility in water, which also proves the successful decoration of CNTs by TA. The zeta potential is an important index for characterizing the stability of a dispersed system and system could be steady when absolute value of potential was greater than 30 mV.<sup>35</sup> The average potential value of TCNTs is about -36.2 mV (Fig. 2c), which demon-

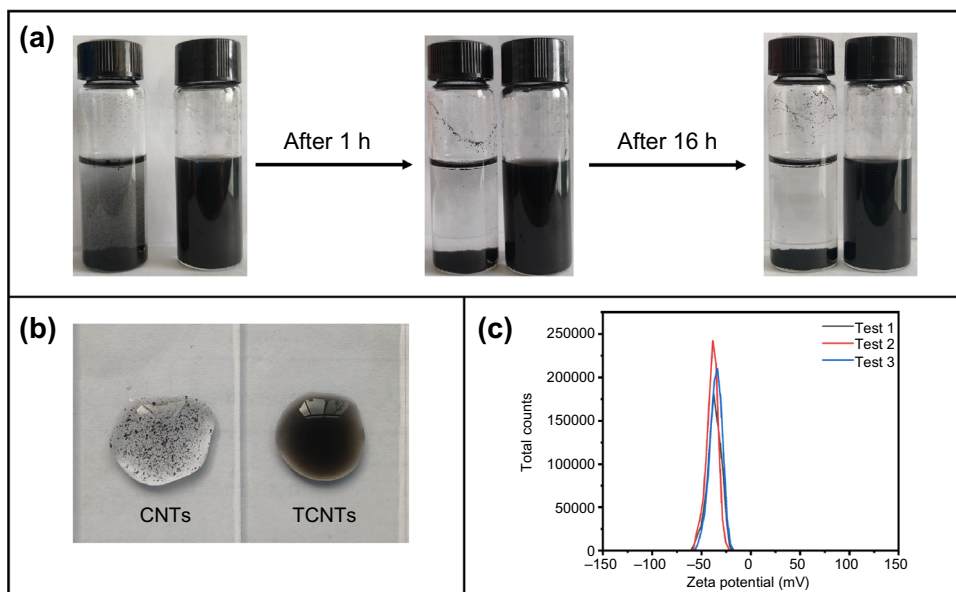


**Fig. 2:** (a) the sedimentation tests of CNTs and TCNTs in water, (b) dispersibility of CNTs and TCNTs in water, (c) zeta potential of TCNTs water dispersion

**Table 1: Surface chemical composition of CNTs and TCNTs hybrids**

	[O]/at%	[C]/at%	[O]/[C]
CNTs	1.90%	98.10%	0.019
TCNTs	10.74%	89.26%	0.120

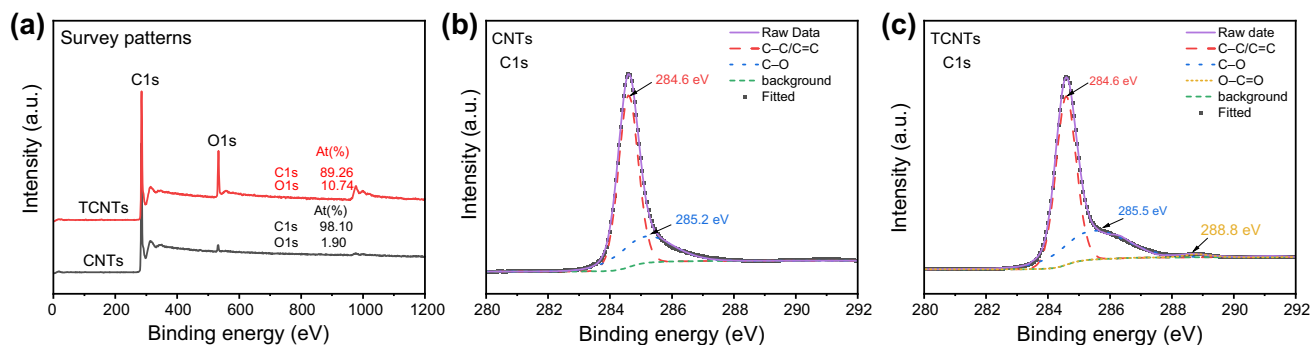


**Fig. 3:** XPS spectra of CNTs and TCNTs hybrids. (a) XPS survey patterns, (b) C1s XPS spectra of CNTs, (c) C1s XPS spectra of TCNTs hybrids

states that TCNTs could exist stably in water. The above results show that the TCNTs dispersion system is a physically stable system.

The XPS spectra of CNTs and TCNTs hybrids are displayed in Fig. 3. As shown in Fig. 3a, wide spectra reveal that carbon and oxygen are the dominant elements on the surface of the CNTs and TCNTs hybrids. Compared with CNTs, the relative intensity of O of TCNTs has a remarkable increase and the elemental ratio of oxygen to carbon for the TCNTs hybrids is six times higher than that of the CNTs (from 0.019 to 0.120, Table 1). In the high-resolution C1s XPS

spectra of CNTs and TCNTs hybrids (Fig. 3b, c), CNTs exhibit two peaks at 284.6 eV and 285.2 eV, corresponding to the C-C/C=C, C-O, respectively.<sup>36,37</sup> For the TCNTs hybrids, however, a new peak occurs at 288.8 eV, which is related with O-C=O.<sup>36</sup> The O-C=O bond is derived from TA molecules via  $\pi$ - $\pi$  interaction. The results show the successful modification of TA.

The TGA was employed to get more information for the decoration of CNTs. Figure 4a shows the TG curves of CNTs and TCNTs in the temperature range from 20 to 800°C. The weight loss percentage of CNTs is observed to be 5% when the temperature is up to

800°C. However, the mass loss of TCNTs hybrids is calculated to be 11% in the range of 20°C to 800°C. The DTG curves also indicate that the temperature of maximum mass loss for TCNTs hybrids is 280°C, which is attributed to the decomposition of TA molecules.<sup>14</sup> The above analysis also confirms the successful functionalization of CNTs with TA and the mass percentage of TA absorbed on the surface of CNTs is calculated to be 6% for TCNTs hybrids.

Figure 5a shows the crystal phase of CNTs and TCNTs hybrids. It is seen that the characteristic peaks of CNTs are at  $2\theta = 25.9^\circ$  and  $43.0^\circ$ , which are associated with the reflections of the in-plane regularity and interlayer spacing of graphite-like structure corresponding to (0 0 2) and (1 0 0) lattice planes.<sup>38,39</sup> The TCNTs hybrids also display same peaks, which

may indicate that the decoration of TA has no effect on the crystal structure of CNTs.

The Raman spectra of CNTs and TCNTs hybrids are displayed in Fig. 5b. The CNTs show two characteristic peaks at 1349 and 1578  $\text{cm}^{-1}$ , which are ascribed to D and G band, respectively. Among them, the D band corresponded to the  $A_{1g}$  vibrational mode of  $sp^3$  C atoms related to surface defects and disorder present in the CNTs,<sup>40,41</sup> the G band associated with the  $E_{2g}$  vibrational mode of  $sp^2$  C atoms which reflects the symmetry of graphite layers in CNTs.<sup>42,43</sup> The G band of CNTs is displaced from 1578 to 1582  $\text{cm}^{-1}$  following TA treatment, confirming the existence of  $\pi$ - $\pi$  interaction between CNTs and TA. Usually, the intensity ratio of D-band to G-band ( $I_D/I_G$ ) could be employed to assess the degree of defects existing on the CNTs.

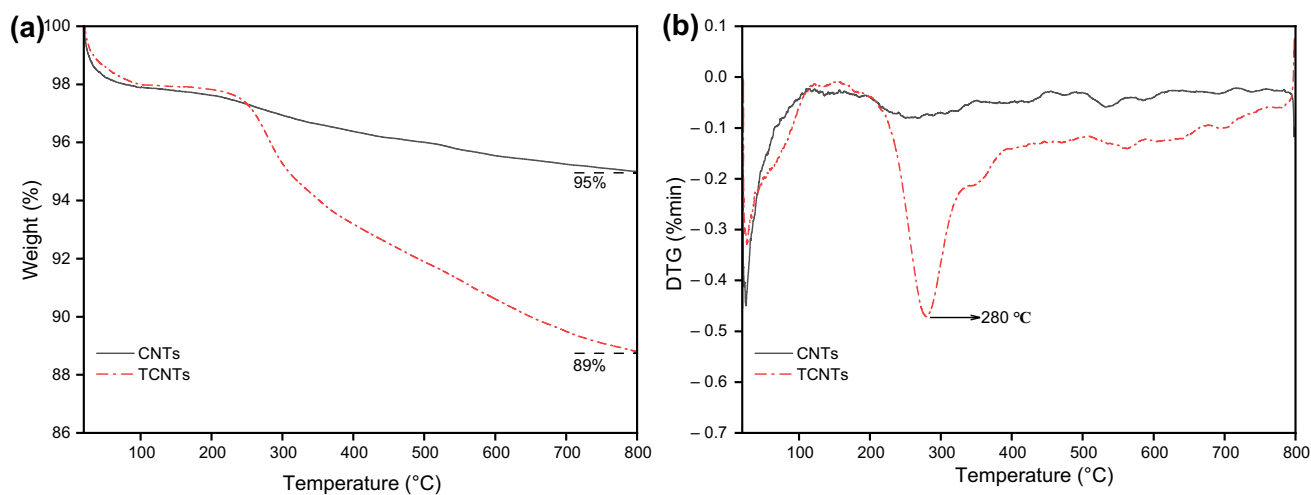


Fig. 4: (a) TG and (b) DTG curves of CNTs and TCNTs hybrids

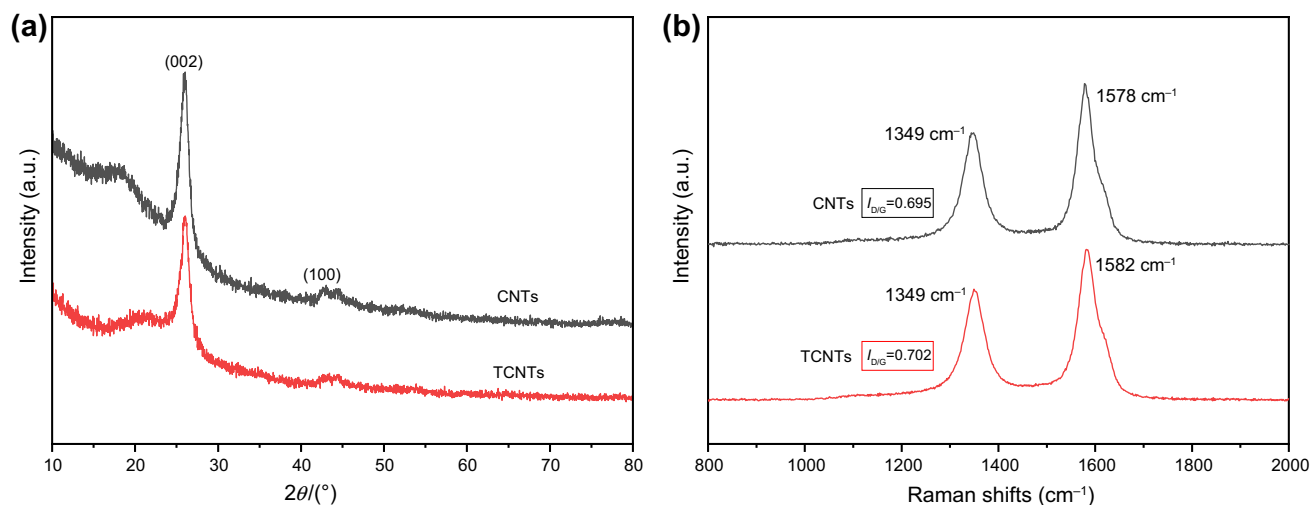


Fig. 5: (a) XRD patterns and (b) Raman spectra of CNTs and TCNTs hybrids



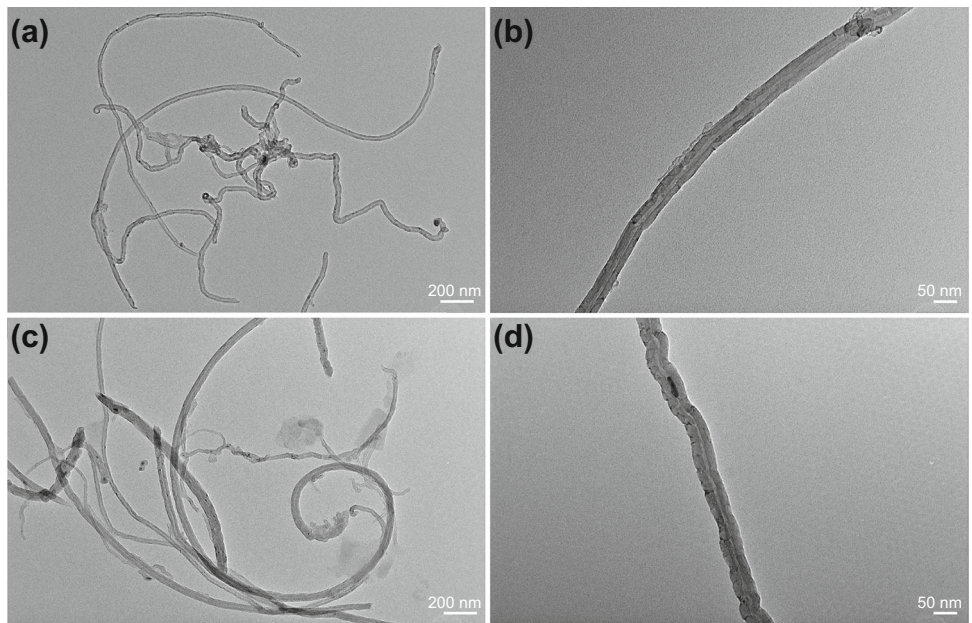


Fig. 6: TEM images of (a, b) CNTs and (c, d) TCNTs hybrids

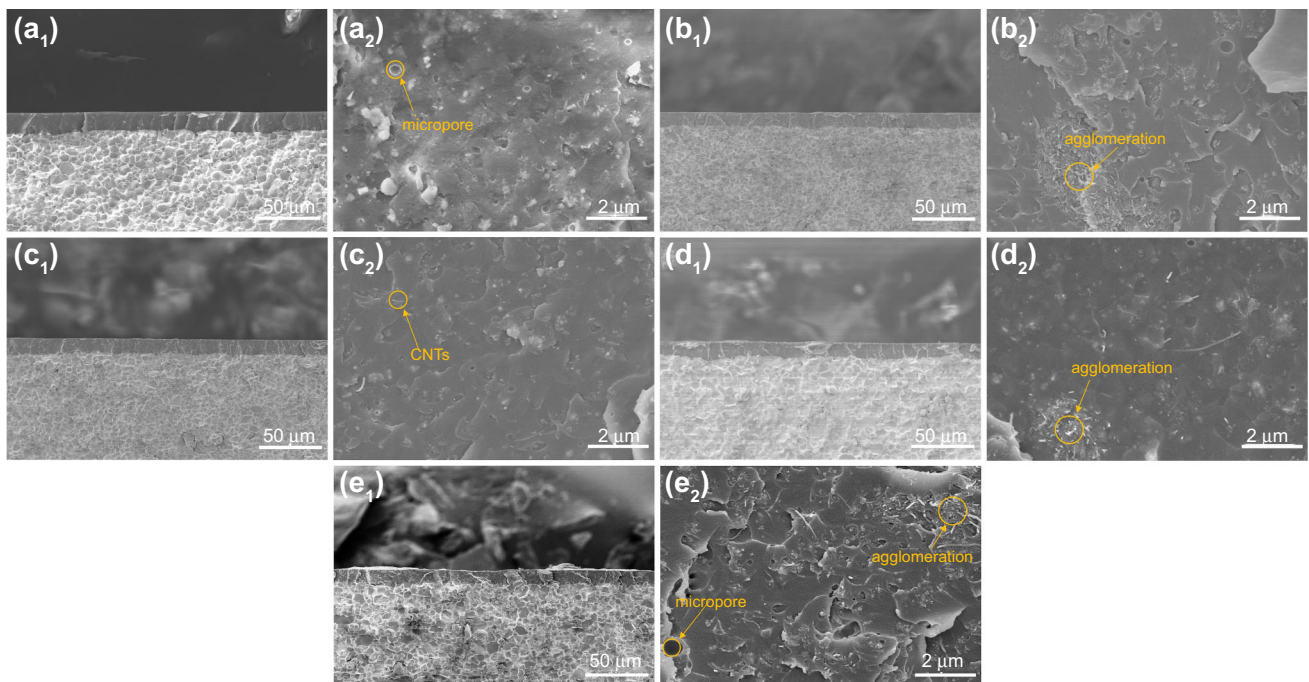


Fig. 7: SEM images of (a) EP, (b) EP/CNTs<sub>2</sub>, (c) EP/TCNTs<sub>2</sub>, (d) EP/TCNTs<sub>5</sub>, and (e) EP/TCNTs<sub>10</sub>

Here, the  $I_D/I_G$  value is 0.695 and 0.702 for CNTs and TCNTs hybrids, respectively; their similar ratios may indicate that the decoration process is moderate and noncovalent, without damaging the original graphene structures of CNTs.

TEM was employed to monitor the morphology and microstructure of CNTs and TCNTs hybrids. As shown in Fig. 6a, 6b, the diameter of CNTs is about 30–50 nm and the length is about 0.5–2 μm. As shown in Fig. 6c, d, there are no obvious changes on the morphology of

CNTs after being treated by TA. This also suggests that TA molecules envelope on the CNTs surface in a single layer, which is consistent with the literature reported.<sup>31</sup>

### Characterization of specimens

#### Cross section morphologies of coatings

The cross section morphologies of the EP, EP/CNTs and EP/TCNTs were observed by SEM (Fig. 7), which revealed the coating thickness and dispersion of CNTs and TCNTs hybrids in epoxy coatings. The coating thickness of EP, EP/CNTs and EP/TCNTs is observed to be 13–16  $\mu\text{m}$  as shown in Fig. 7a<sub>1</sub>–e<sub>1</sub>, which illustrates that the addition of CNTs has no obvious effect on the thickness of the epoxy coatings on NdFeB magnets within the concentration of 10 g/L. Moreover, there is no evident disruption between the coatings and magnets, suggesting that all coatings have good interfacial linkage with NdFeB magnets.

Figure 7a<sub>2</sub>–e<sub>2</sub> shows the detailed morphologies of the coatings. As shown in Fig. 7a<sub>2</sub>, pure epoxy coatings present a relatively smooth cross section morphology. But there are abundant micropores in the coating with size of 0.04–0.35  $\mu\text{m}$  because of the high-speed evaporation of water in solidification process. Therefore, it is necessary to incorporate nanomaterials to fill in the micropores and extend the invasion channel of corrosive media inside the coatings. Compared with the pure epoxy coatings, the cross section of the EP/CNTs and EP/TCNTs system exhibits completely different morphologies, which have an irregular cross-sectional morphology due to the presence of CNTs. As shown in Fig. 7b<sub>2</sub>, the serious agglomerated CNTs are observed, which is ascribed to the poor dispersion of pristine CNTs in epoxy coatings and will bring about side effects on anticorrosion performance of coatings. Compared with pristine CNTs, the TCNTs hybrids display more uniform dispersal in the epoxy coatings at the same concentration (Fig. 7c<sub>2</sub>), which will endow the coatings a better barrier property to corrosive media. However, with the increasing content of TCNTs hybrids (Fig. 7d<sub>2</sub>, e<sub>2</sub>), the agglomeration can be clearly seen in the coatings again. Especially in EP/TCNTs<sub>10</sub> system, there are many serious agglomerations and result in a large number of micropore defects, which may indicate that the coating has poor resistance to corrosive media.

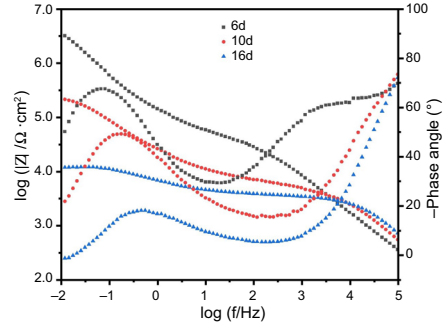
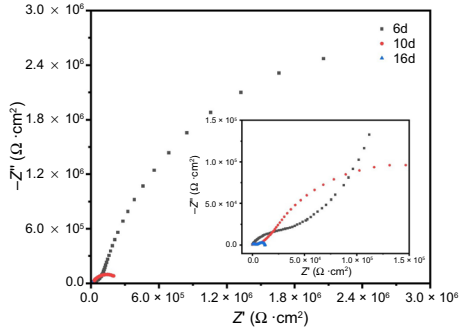
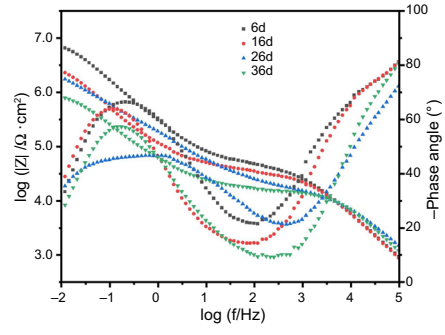
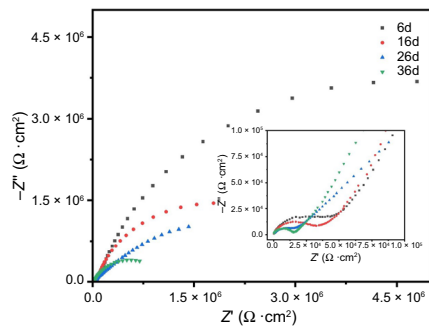
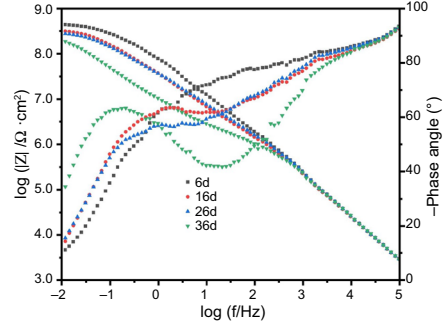
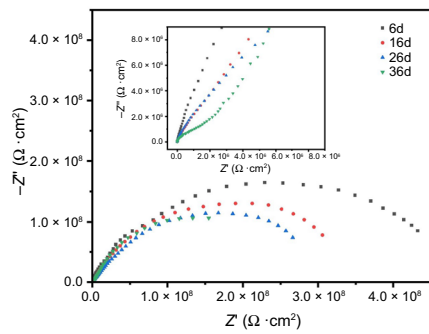
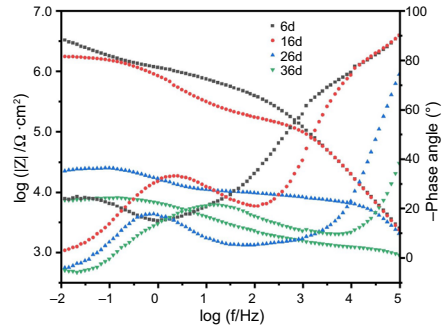
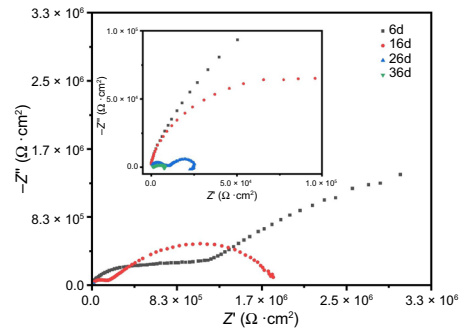
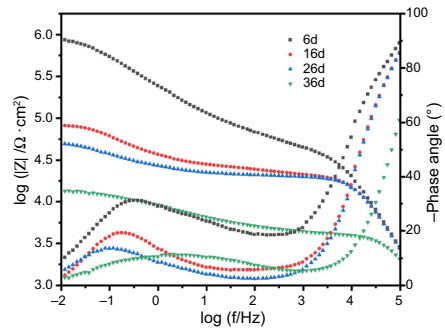
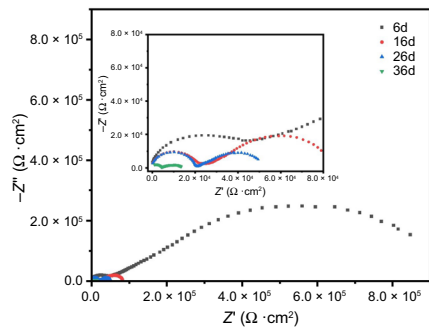
#### Electrochemical corrosion properties of specimens

As shown in Fig. 8, the EIS plots of the sintered NdFeB magnets covered by epoxy coatings in 3.5 wt.% NaCl solution for certain time are presented. As shown in Fig. 8a<sub>1</sub>–e<sub>1</sub>, all specimens display two arcs during initial immersion process except EP/TCNTs<sub>2</sub>. Generally, the time constant in the high frequency zone is associated

with the coating response, and the time constant in the low and medium frequency areas corresponds to the corrosion response of metal matrix.<sup>44</sup> When the second time constant appears, it indicates that the corrosion media has reached the coating/substrate interface. For EP/TCNTs<sub>2</sub>, the second time constant appears after soaking for 26 days, which shows excellent barrier properties to corrosive media. It is known that a higher radius of the capacitive impedance arc in the Nyquist plot suggests a better barrier properties of coating.<sup>45</sup> At the beginning of immersion, the arc radius of all composite specimens is larger than that of pristine EP specimen, suggesting that the addition of CNTs increases the coating impedance. It is noteworthy that with the prolong of soaking time, the arc radius of EP/CNTs<sub>2</sub> and EP/TCNTs<sub>10</sub> specimens is gradually smaller than EP specimen. While for EP/TCNTs<sub>2</sub> and EP/TCNTs<sub>5</sub>, the arc radius is always higher than other specimens, which demonstrates that the specimens possess better resistance to corrosion.

Usually, the low-frequency impedance modulus ( $|Z|_{0.01\text{Hz}}$ ) in the Bode plot is a semiquantitative index to evaluate coating's shielding performance, and the higher  $|Z|_{0.01\text{Hz}}$  value at low-frequency zone represent the more outstanding anticorrosion properties of specimens.<sup>11,46</sup> Figure 8a<sub>2</sub>–e<sub>2</sub> shows the Bode plots of prepared specimens and  $|Z|_{0.01\text{Hz}}$  of the specimens after different times exposure to 3.5 wt.% NaCl solution are listed in Table 2. As can be seen, the impedance modulus are  $8.60 \times 10^5 \Omega \text{ cm}^2$ ,  $3.29 \times 10^6 \Omega \text{ cm}^2$ ,  $4.41 \times 10^8 \Omega \text{ cm}^2$ ,  $6.53 \times 10^6 \Omega \text{ cm}^2$ , and  $3.22 \times 10^6 \Omega \text{ cm}^2$ , respectively, for EP, EP/CNTs<sub>2</sub>, EP/TCNTs<sub>2</sub>, EP/TCNTs<sub>5</sub>, and EP/TCNTs<sub>10</sub> specimens soaked in 3.5 wt.% NaCl solution for 6 days, suggesting the composite specimens' superior barrier properties than that of pure EP specimen during initial stage. However, the  $|Z|_{0.01\text{Hz}}$  decrease to  $1.19 \times 10^4 \Omega \text{ cm}^2$  for EP/TCNTs<sub>10</sub> after exposure to 3.5 wt.% NaCl solution for 16 days, which is even lower than that of EP after immersing for 36 days ( $1.34 \times 10^4 \Omega \text{ cm}^2$ ). For EP/CNTs<sub>2</sub> system, the  $|Z|_{0.01\text{Hz}}$  displays a drastic reduction from  $1.76 \times 10^6$  to  $2.27 \times 10^4 \Omega \text{ cm}^2$  (from 16 days to 26 days) and is lower than that of the EP at 26 days. What is delightful is that the EP/TCNTs<sub>2</sub> system's  $|Z|_{0.01\text{Hz}}$  has been kept at  $\sim 10^8 \Omega \text{ cm}^2$  within 36 days, which means it has more excellent barrier properties. And for EP/TCNTs<sub>5</sub> system, its  $|Z|_{0.01\text{Hz}}$  gradually decreases from  $6.53 \times 10^6$  to  $7.92 \times 10^5 \Omega \text{ cm}^2$  within 36 days, which is better than other systems except EP/TCNTs<sub>2</sub>. To sum up, EP/TCNTs<sub>2</sub> and EP/TCNTs<sub>5</sub> specimens have better resistance to corrosive media than other specimens as optimized specimen.

Figure 9 shows the potentiodynamic polarization curves of different specimens after 40 days soaking in 3.5 wt.% NaCl (The  $|Z|_{0.01\text{Hz}}$  of EP/TCNTs<sub>10</sub> immersed in 3.5 wt.% NaCl for 16 days is lower than EP for 36 days, so no further test is required for EP/TCNTs<sub>10</sub>), and corresponding polarization parameters are presented in Table 3. Furthermore, the potentiodynamic polarization curve of pristine NdFeB magnet immersed





◀ **Fig. 8: Nyquist and Bode plots of different coating systems in 3.5 wt.% NaCl solution. (a) EP, (b) EP/CNTs<sub>2</sub>, (c) EP/TCNTs<sub>2</sub>, (d) EP/TCNTs<sub>5</sub>, (e) EP/TCNTs<sub>10</sub>**

in 3.5 wt.% NaCl for 1 h is also shown for comparison. Generally,  $E_{\text{corr}}$  represents a sample's susceptibility to corrosion, while the anodic dissolution of metal ions and intensity of the cathodic oxygen reduction is usually expressed by  $J_{\text{corr}}$ , and more positive  $E_{\text{corr}}$  and lower  $J_{\text{corr}}$  indicates better corrosion resistance.<sup>47</sup> For pristine NdFeB magnets, the  $E_{\text{corr}}$  is  $-0.929$  V and the highest  $J_{\text{corr}}$  is  $2.302 \times 10^{-5} \text{ A cm}^{-2}$  after 1 h immersion, illustrating that the intrinsic corrosion resistance of magnets is poor. In contrast, the EP exhibits lower  $J_{\text{corr}} = 4.436 \times 10^{-6} \text{ A cm}^{-2}$  and positive shifts of  $E_{\text{corr}}$  to  $-0.816$  V after 40 days of soaking in 3.5 wt.% NaCl, indicating the better anticorrosion performance. When the CNTs with a concentration of 2 g/L were directly introduced into the coating, the polarization results are similar to EP with  $E_{\text{corr}} = -0.815$  V and  $J_{\text{corr}} = 3.846 \times 10^{-6} \text{ A cm}^{-2}$ , which demonstrates that the introduction of original CNTs cannot promote the anticorrosion properties of specimens due to the bad coating quality. By addition of TCNTs hybrids, the  $E_{\text{corr}}$  shifts to a more positive position, which is  $-0.314$  V for EP/TCNTs<sub>5</sub> and  $-0.207$  V for EP/TCNTs<sub>2</sub>. In the meantime,  $J_{\text{corr}}$  decreases to  $2.792 \times 10^{-8} \text{ A cm}^{-2}$  and  $5.281 \times 10^{-11} \text{ A cm}^{-2}$ , respectively. Obviously, the composite specimens prepared by adding TCNTs hybrids could effectively improve the corrosion resistance. Then, EP/TCNTs<sub>2</sub> specimens exhibit the lowest corrosion current density, thus it can be concluded that it possesses the best corrosion performance.

The improved corrosion resistance of the specimens is mainly ascribed to the good water dispersibility of TCNTs, which can achieve good dispersion in polymer matrix. But this can also be achieved by chemical oxidation of CNTs. Here, we compared the corrosion protection data of chemical oxidized CNTs enhanced epoxy coatings with this work. As shown in Table 4, corrosion resistance of our specimens is better than that of the specimens in most references<sup>48–51</sup> except Ref. 38. But considering the difference in coatings' thickness and the noncovalent method is easier, more eco-friendly and does no damage on the original

structure of CNTs, our work still has its potential advantages.

Static immersion corrosion test was employed to assess the optimized specimens' resistance to corrosion. As shown in Fig. 10a<sub>1</sub>–c<sub>1</sub>, the EP is seriously corroded and bulged after immersed in 3.5 wt.% NaCl solution for 40 days. The surface of EP/TCNTs<sub>5</sub> appears dense bulge while there is no change on the surface of EP/TCNTs<sub>2</sub>. When the soaking time is prolonged to 50 days (shown in Fig. 10a<sub>2</sub>–c<sub>2</sub>), the corrosion area of EP continues to expand, a small bulge appears in the corner of EP/TCNTs<sub>2</sub>, and corrosion products appear on the surface of EP/TCNTs<sub>5</sub>.

The above results are consistent with the electrochemical experiments that EP/TCNTs<sub>2</sub> and EP/TCNTs<sub>5</sub> possess better corrosion resistance of prepared specimens.

### Corrosion protection mechanism

According to the above discussion, we can deduce that the corrosion-resisting performance of specimens can be improved by incorporating TCNTs hybrids in epoxy coatings and the possible protective mechanism is

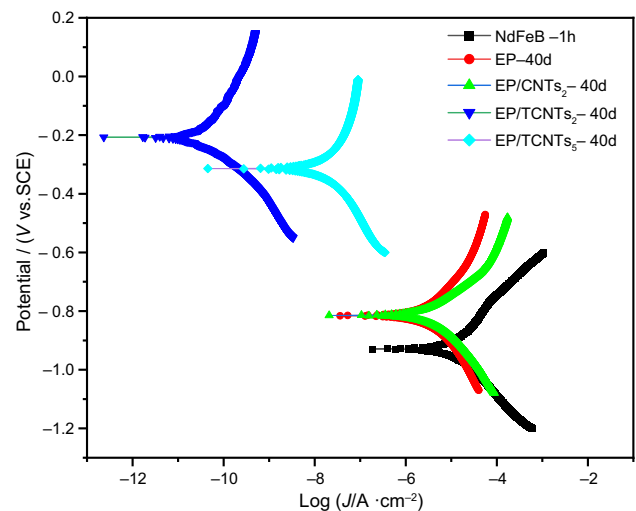


**Fig. 9: Potentiodynamic polarization curves of different specimens after being immersed in 3.5 wt.% NaCl for 40 days**

**Table 2:  $|Z|_{0.01\text{Hz}}$  of specimens after being immersed in 3.5 wt.% NaCl solution for different times**

Time	EP	EP/CNTs <sub>2</sub>	EP/TCNTs <sub>2</sub>	EP/TCNTs <sub>5</sub>	EP/TCNTs <sub>10</sub>
6d	$8.60 \times 10^5$	$3.29 \times 10^6$	$4.41 \times 10^8$	$6.53 \times 10^6$	$3.22 \times 10^6$
16d	$8.19 \times 10^4$	$1.76 \times 10^6$	$3.16 \times 10^8$	$2.30 \times 10^6$	$1.19 \times 10^4$
26d	$4.96 \times 10^4$	$2.27 \times 10^4$	$2.77 \times 10^8$	$1.74 \times 10^6$	–
36d	$1.34 \times 10^4$	$7.42 \times 10^3$	$1.88 \times 10^8$	$7.92 \times 10^5$	–

**Table 3: Electrochemical polarization parameters of different specimens**

Sample	$J_{corr}$ (A cm <sup>-2</sup> )	$E_{corr}$ (V)	$-\beta_c$ (V/dec)	$\beta_a$ (V/dec)
NdFeB-1h	$2.302 \times 10^{-5}$	- 0.929	0.162	0.197
EP-40d	$4.436 \times 10^{-6}$	- 0.816	0.173	0.166
EP/CNT <sub>S2</sub> -40d	$3.846 \times 10^{-6}$	- 0.815	0.157	0.109
EP/TCNT <sub>S2</sub> -40d	$5.281 \times 10^{-11}$	- 0.207	0.116	0.195
EP/TCNT <sub>S5</sub> -40d	$2.792 \times 10^{-8}$	- 0.314	0.182	0.237

**Table 4: Comparison of corrosion protection data of chemical oxidized CNTs enhanced epoxy coatings with this work**

Electrolyte	Thickness of coating (μm)	$ Z _{0.01Hz}$ (Ω cm <sup>2</sup> )	$E_{corr}$ (V)	$J_{corr}$ (A cm <sup>-2</sup> )	Reference
3.5 wt.% NaCl	200 ± 35	-	- 0.31 (7d)	$5.9 \times 10^{-10}$ (7d)	Ref. 48
3.5 wt.% NaCl	25	$10^5$ - $10^6$ (unknown)	- 0.148 (unknown)	$6.030 \times 10^{-6}$ (unknown)	Ref. 49
0.5 M NaCl	20	$10^5$ - $10^6$ (1d)	-	-	Ref. 50
3.5 wt.% NaCl	110 ± 10	$1.2 \times 10^4$ (7d)	- 0.508 (1h)	$1.393 \times 10^{-7}$ (1h)	Ref. 51
3.5 wt.% NaCl	70	$2.51 \times 10^{10}$ (35d)	-	-	Ref. 38
3.5 wt.% NaCl	13–16	$1.88 \times 10^8$ (36d)	- 0.207 (40d)	$5.281 \times 10^{-11}$ (40d)	This work

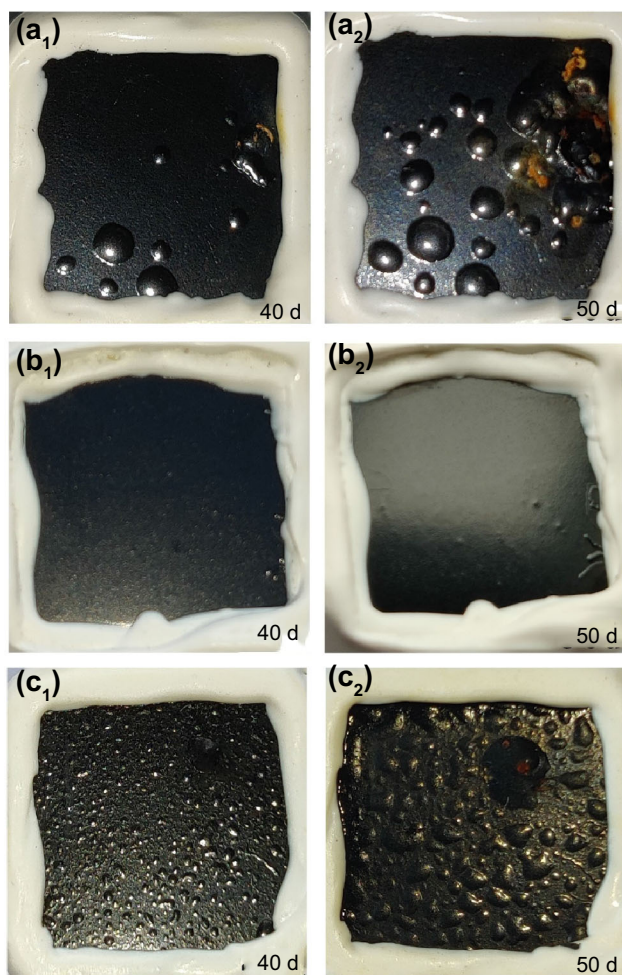


**Fig. 10: The surface images of (a) EP, (b) EP/TCNT<sub>S2</sub>, (c) EP/TCNT<sub>S5</sub> immersed in 3.5 wt.% NaCl solution**

discussed as follows. In the case of EP system (Fig. 11a), the internal defects, including micropores inevitably formed due to the water evaporation during the solidification process of coating, will become the invasion channel of corrosive media. A series of electrochemical and redox reactions happens when corrosive media such as H<sub>2</sub>O, O<sub>2</sub>, and Cl<sup>-</sup> reach to the coating/substrate interface, and result in the failure of specimens. For EP/CNTs specimen (Fig. 11b), the addition of nano-fillers should have filled the defects of coating to promote its barrier ability to the corrosion medium, but the anticorrosion performance of the composite specimens did not improve due to the poor dispersion of CNTs in epoxy resin. However, in terms of EP/TCNTs specimen (Fig. 11c), with the hydrophilic TA absorbed on the surface, the dispersion of TCNTs in epoxy coating is greatly improved compared with pristine CNTs. Thus, the corrosion resistance of EP/TCNTs specimen has been obviously improved due to the less defects in the coating and increased invasion channel of corrosive media produced by TCNTs hybrids.

### Conclusions

In the present work, TCNTs hybrids are obtained through π-π noncovalent modification, which exhibit better water dispersibility than pure CNTs due to the absorption of hydrophilic TA. The TCNTs enhanced epoxy composite coatings are prepared by cathodic electrophoretic deposition method and applied on NdFeB magnets. Electrochemical tests demonstrate that the corrosion resistance of EP/TCNTs specimens are improved obviously compared with the pure EP

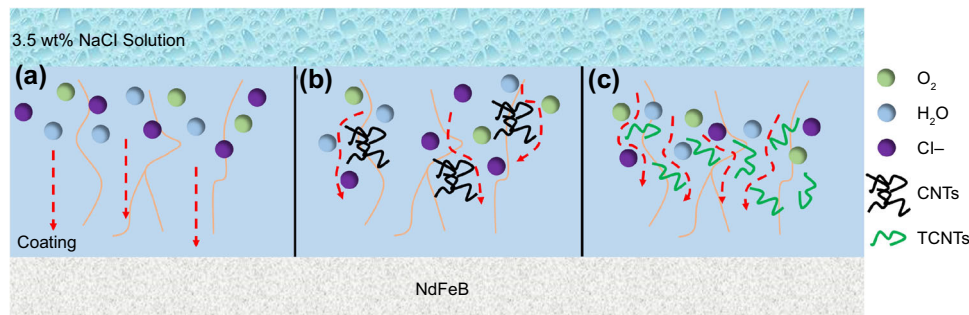


Fig. 11: Corrosion protection mechanism for (a) EP, (b) EP/CNTs, (c) EP/TCNTs

and EP/CNTs specimens. Under optimized conditions, the EP/TCNTs<sub>2</sub> achieve a  $J_{\text{corr}} = 5.281 \times 10^{-11} \text{ A cm}^{-2}$  after 40 days soaking in 3.5 wt.% NaCl solution. The significant improvement in anticorrosion properties of EP/TCNTs<sub>2</sub> specimens is probably due to the homogenous dispersion of TCNTs hybrids in epoxy matrix, which can availablely fill the defects in epoxy matrix and extend the invasion channel of corrosive media, thus delaying the failure of specimens.

**Acknowledgments** This work was financially supported by the Key Project of BGRIMM Technology Group Co. Ltd (20190898000002), Hefei Municipal Natural Science Foundation (2021026), the Key Research and Development Project of Anhui Province (202004a05020048, 202004a05020051), and the Fundamental Research Funds for the Central Universities (JZ2019HGBZ0142, PA2019GDPK0043, PA2020GDJQ0026).

## References

- Fidler, J, Schrefl, T, Hoefinger, S, Hajduga, M, "Recent Developments in Hard Magnetic Bulk Materials." *J. Phys. Condens. Matter*, **16** (5) S455–S470 (2004)
- Matsuura, Y, "Recent Development of Nd-Fe-B Sintered Magnets and Their Applications." *J. Magn. Magn. Mater.*, **303** (2) 344–347 (2006)
- Sagawa, M, Fujimura, S, Togawa, N, Yamamoto, H, Matsuura, Y, "New Material for Permanent Magnets on a Base of Nd and Fe (Invited)." *J. Appl. Phys.*, **55** (6) 2083–2087 (1984)
- Yan, G, Williams, AJ, Farr, JPG, Harris, IR, "The Effect of Density on the Corrosion of NdFeB Magnets." *J. Alloys Compd.*, **292** (1) 266–274 (1999)
- Schultz, L, El-Aziz, AM, Barkleit, G, Mummert, K, "Corrosion Behaviour of Nd-Fe-B Permanent Magnetic Alloys." *Mater. Sci. Eng. A*, **267** (2) 307–313 (1999)
- Dai, J, Yang, Z, Liu, Q, "Rare Earth Cerium Increases the Corrosion Resistance of NdFeB Magnets." *Materials*, **13** (19) 4360 (2020)
- Chen, W, Huang, YL, Luo, JM, Hou, YH, Ge, XJ, Guan, YW, Liu, ZW, Zhong, ZC, Wang, GP, "Microstructure and Improved Properties of Sintered Nd-Fe-B Magnets by Grain Boundary Diffusion of Non-rare Earth." *J. Magn. Magn. Mater.*, **476** 134–141 (2019)
- Yu, LQ, Wen, YH, Yan, M, "Effects of Dy and Nb on the Magnetic Properties and Corrosion Resistance of Sintered NdFeB." *J. Magn. Magn. Mater.*, **283** (2) 353–356 (2004)
- Sun, C, Liu, WQ, Sun, H, Yue, M, Yi, XF, Chen, JW, "Improvement of Coercivity and Corrosion Resistance of Nd-Fe-B Sintered Magnets with Cu Nano-particles Doping." *J. Mater. Sci. Technol.*, **28** (10) 927–930 (2012)
- Isotahdon, E, Huttunen-Saarivirta, E, Kuokkala, VT, Paju, M, "Corrosion Behaviour of Sintered Nd-Fe-B Magnets." *Mater. Chem. Phys.*, **135** (2) 762–771 (2012)
- Wu, Y, Yu, J, Zhao, W, Wang, C, Wu, B, Lu, G, "Investigating the Anti-corrosion Behaviors of the Waterborne Epoxy Composite Coatings with Barrier and Inhibition Roles on Mild Steel." *Prog. Org. Coat.*, **133** 8–18 (2019)
- Yan, H, Li, W, Li, H, Fan, X, Zhu, M, "Ti<sub>3</sub>C<sub>2</sub> MXene Nanosheets Toward High-Performance Corrosion Inhibitor for Epoxy Coating." *Prog. Org. Coat.*, **135** 156–167 (2019)
- Wu, Y, He, Y, Chen, C, Zhong, F, Li, H, Chen, J, Zhou, T, "Non-covalently Functionalized Boron Nitride by Graphene Oxide for Anticorrosive Reinforcement of Water-Borne Epoxy Coating." *Colloids Surf. A Physicochem. Eng. Asp.*, **587** 124337 (2020)
- He, Y, Chen, C, Xiao, G, Zhong, F, Wu, Y, He, Z, "Improved Corrosion Protection of Waterborne Epoxy/Graphene Coating by Combining Non-covalent and Covalent Bonds." *React. Funct. Polym.*, **137** 104–115 (2019)
- Wu, Y, He, Y, Zhou, T, Chen, C, Zhong, F, Xia, Y, Xie, P, Zhang, C, "Synergistic Functionalization of h-BN by Mechanical Exfoliation and PEI Chemical Modification for Enhancing the Corrosion Resistance of Waterborne Epoxy Coating." *Prog. Org. Coat.*, **142** 105541 (2020)
- Yu, D, Wen, S, Yang, J, Wang, J, Chen, Y, Luo, J, Wu, Y, "RGO Modified ZnAl-LDH as Epoxy Nanostructure Filler: A Novel Synthetic Approach to Anticorrosive Waterborne Coating." *Surf. Coat. Technol.*, **326** 207–215 (2017)
- Yan, H, Li, J, Zhang, M, Zhao, Y, Feng, Y, Zhang, Y, "Enhanced Corrosion Resistance and Adhesion of Epoxy Coating by Two-Dimensional Graphite-Like g-C<sub>3</sub>N<sub>4</sub> Nanosheets." *J. Colloid Interface Sci.*, **579** 152–161 (2020)
- Huang, H, Li, M, Tian, Y, Xie, Y, Sheng, X, Jiang, X, Zhang, X, "Exfoliation and Functionalization of  $\alpha$ -Zirconium Phosphate in One Pot for Waterborne Epoxy Coatings with Enhanced Anticorrosion Performance." *Prog. Org. Coat.*, **138** 105390 (2020)
- Liu, T, Liu, Y, Ye, Y, Li, J, Yang, F, Zhao, H, Wang, L, "Corrosion Protective Properties of Epoxy Coating Containing Tetraaniline Modified Nano- $\alpha$ -Fe<sub>2</sub>O<sub>3</sub>." *Prog. Org. Coat.*, **132** 455–467 (2019)



20. Wang, N, Gao, H, Zhang, J, Li, L, Fan, X, Diao, X, “Anticorrosive Waterborne Epoxy (EP) Coatings Based on Sodium Tripolyphosphate-Pillared Layered Double Hydroxides (STPP-LDHs).” *Prog. Org. Coat.*, **135** 74–81 (2019)
21. Khodabakhshi, J, Mahdavi, H, Najafi, F, “Investigation of Viscoelastic and Active Corrosion Protection Properties of Inhibitor Modified Silica Nanoparticles/Epoxy Nanocomposite Coatings on Carbon Steel.” *Corros. Sci.*, **147** 128–140 (2019)
22. Gu, L, Liu, S, Zhao, H, Yu, H, “Facile Preparation of Water-Dispersible Graphene Sheets Stabilized by Carboxylated Oligoanilines and Their Anticorrosion Coatings.” *ACS Appl. Mater. Interfaces*, **7** (32) 17641–17648 (2015)
23. Chen, J, Zhao, W, “Silk Fibroin-Ti<sub>3</sub>C<sub>2</sub>T<sub>x</sub> Hybrid Nanofiller Enhance Corrosion Protection for Waterborne Epoxy Coatings Under Deep Sea Environment.” *Chem. Eng. J.*, **423** 130195 (2021)
24. Pop, E, Mann, D, Wang, Q, Goodson, K, Dai, H, “Thermal Conductance of an Individual Single-Wall Carbon Nanotube Above Room Temperature.” *Nano Lett.*, **6** (1) 96–100 (2006)
25. Sanli, A, Benchirouf, A, Müller, C, Kanoun, O, “Piezoresistive Performance Characterization of Strain Sensitive Multi-walled Carbon Nanotube-Epoxy Nanocomposites.” *Sens. Actuators A Phys.*, **254** 61–68 (2017)
26. Moaseri, E, Karimi, M, Baniadam, M, Maghrebi, M, “Improvements in Mechanical Properties of Multi-walled Carbon Nanotube-Reinforced Epoxy Composites Through Novel Magnetic-Assisted Method for Alignment of Carbon Nanotubes.” *Compos. Part A Appl. Sci. Manuf.*, **64** 228–233 (2014)
27. Liao, W-H, Tien, H-W, Hsiao, S-T, Li, S-M, Wang, Y-S, Huang, Y-L, Yang, S-Y, Ma, C-CM, Wu, Y-F, “Effects of Multiwalled Carbon Nanotubes Functionalization on the Morphology and Mechanical and Thermal Properties of Carbon Fiber/Vinyl Ester Composites.” *ACS Appl. Mater. Interfaces*, **5** (9) 3975–3982 (2013)
28. Ma, P-C, Siddiqui, N, Marom, G, Kim, J-K, “Dispersion and Functionalization of Carbon Nanotubes for Polymer-Based Nanocomposites: A Review.” *Compos. Part A Appl. Sci. Manuf.*, **41** 1345–1367 (2010)
29. Deyab, MA, Awadallah, AE, “Advanced Anticorrosive Coatings Based on Epoxy/Functionalized Multiwall Carbon Nanotubes Composites.” *Prog. Org. Coat.*, **139** 105423 (2020)
30. Cui, M, Ren, S, Qiu, S, Zhao, H, Wang, L, Xue, Q, “Non-covalent Functionalized Multi-wall Carbon Nanotubes Filled Epoxy Composites: Effect on Corrosion Protection and Tribological Performance.” *Surf. Coat. Technol.*, **340** 74–85 (2018)
31. Jin, YN, Yang, HC, Huang, H, Xu, ZK, “Underwater Superoleophobic Coatings Fabricated from Tannic Acid-Decorated Carbon Nanotubes.” *Rsc Adv.*, **5** (21) 16112–16115 (2015)
32. Lin, DH, Xing, BS, “Tannic Acid Adsorption and Its Role for Stabilizing Carbon Nanotube Suspensions.” *Environ. Sci. Technol.*, **42** (16) 5917–5923 (2008)
33. Shi, L, Zhang, D, Zhao, J, Yin, M, Liang, A, Ghosh, S, “Small Organic Molecules Act as a Trigger in an ‘Unzippering’ Mechanism to Facilitate Carbon Nanotube Dispersion.” *Sci. Total Environ.*, **758** 143620 (2021)
34. He, P, Wu, JY, Pan, XF, Chen, LH, Liu, K, Gao, HL, Wu, H, Cao, SL, Huang, LL, Ni, YH, “Anti-freezing and Moisturizing Conductive Hydrogels for Strain Sensing and Moist-Electric Generation Applications.” *J. Mater. Chem. A*, **8** (6) 3109–3118 (2020)
35. Wang, S, Hu, Z, Shi, J, Chen, G, Zhang, Q, Weng, Z, Wu, K, Lu, M, “Green Synthesis of Graphene with the Assistance of Modified Lignin and Its Application in Anticorrosive Waterborne Epoxy Coatings.” *Appl. Surf. Sci.*, **484** 759–770 (2019)
36. Zheng, X, Xu, J, Yan, K, Wang, H, Wang, Z, Yang, S, “Space-Confined Growth of MoS<sub>2</sub> Nanosheets within Graphite: The Layered Hybrid of MoS<sub>2</sub> and Graphene as an Active Catalyst for Hydrogen Evolution Reaction.” *Chem. Mater.*, **26** (7) 2344–2353 (2014)
37. Zhu, L, Feng, C, Cao, Y, “Corrosion Behavior of Epoxy Composite Coatings Reinforced with Reduced Graphene Oxide Nanosheets in the High Salinity Environments.” *Appl. Surf. Sci.*, **493** 889–896 (2019)
38. Najmi, P, Keshmiri, N, Ramezanzadeh, M, Ramezanzadeh, B, “Synthesis and Application of Zn-Doped Polyaniline Modified Multi-walled Carbon Nanotubes as Stimuli-Responsive Nanocarrier in the Epoxy Matrix for Achieving Excellent Barrier-Self-Healing Corrosion Protection Potency.” *Chem. Eng. J.*, **412** 128637 (2021)
39. Kumar, AM, Rahman, MM, Gasem, ZM, “A Promising Nanocomposite from CNTs and Nanoceria: Nanostructured Fillers in Polyurethane Coatings for Surface Protection.” *Rsc Adv.*, **5** (78) 63537–63544 (2015)
40. Ling, X-L, Wei, Y-Z, Zou, L-M, Xu, S, “Preparation and Characterization of Hydroxylated Multi-walled Carbon Nanotubes.” *Colloids Surf. A Physicochem. Eng. Asp.*, **421** 9–15 (2013)
41. Lee, S, Peng, J-W, Liu, C-H, “Raman Study of Carbon Nanotube Purification Using Atmospheric Pressure Plasma.” *Carbon*, **46** (15) 2124–2132 (2008)
42. Bounos, G, Andrikopoulos, KS, Karachalios, TK, Voyiatzis, GA, “Evaluation of Multi-walled Carbon Nanotube Concentrations in Polymer Nanocomposites by Raman Spectroscopy.” *Carbon*, **76** 301–309 (2014)
43. Chih-Ming, H, Chii-Ruey, L and Jyun-Yan, C, “Raman Spectra Analysis of MWCNTs Based on Empirical Model Decomposition.” *Proc. 2010 IEEE International Conference on Systems, Man and Cybernetics*, 10–13 Oct. (2010)
44. Chen, C, Qiu, S, Cui, M, Qin, S, Yan, G, Zhao, H, Wang, L, Xue, Q, “Achieving High Performance Corrosion and Wear Resistant Epoxy Coatings via Incorporation of Noncovalent Functionalized Graphene.” *Carbon*, **114** 356–366 (2017)
45. Wu, Y, Jiang, F, Qiang, Y, Zhao, W, “Synthesizing a Novel Fluorinated Reduced Graphene Oxide-CeO<sub>2</sub> Hybrid Nanofiller to Achieve Highly Corrosion Protection for Waterborne Epoxy Coatings.” *Carbon*, **176** 39–51 (2021)
46. Conradi, M, Kocijan, A, Kek-Merl, D, Zorko, M, Verpoest, I, “Mechanical and Anticorrosion Properties of Nanosilica-Filled Epoxy-Resin Composite Coatings.” *Applied Surface Science*, **292** 432–437 (2014)
47. Zamani, A, Eavani, S, Rafiee, E, “Synthesis and Characterization of Anticorrosion, Low-Lead Leaching PbCrO<sub>4</sub>/Eggshell Composites as the Environmentally Sustainable Yellow Pigments.” *J. Clean. Prod.*, **304** 127103 (2021)
48. Lorwanishpaisarn, N, Srikhao, N, Jetsrisuparb, K, Knijnenburg, JTN, Theerakulpisut, S, Okhawilai, M, Kasemsiri, P, “Self-Healing Ability of Epoxy Vitriimer Nanocomposites Containing Bio-based Curing Agents and Carbon Nanotubes for Corrosion Protection.” *J. Poly. Environ.*, **30** (2) 472–482 (2022)
49. Raza, MA, Ghauri, FA, Awan, MS, Farooq, A, Ahmad, R, “Production of Carbon Nano-tubes via CCVD Method and Their Corrosion Protection Performance in Epoxy Based Coatings.” *IOP Conf. Ser. Mater. Sci. Eng.*, **146** 012021 (2016)
50. Pham, GV, Trinh, AT, Hang To, TX, Nguyen, TD, Nguyen, TT, Nguyen, XH, “Incorporation of Fe<sub>3</sub>O<sub>4</sub>/CNTs Nanocomposite in an Epoxy Coating for Corrosion Protection of



Carbon Steel.” *Adv. Nat. Sci. Nanosci. Nanotechnol.*, **5** (3) 035016 (2014)

51. Hu, H, He, Y, Long, Z, Zhan, Y, “Synergistic Effect of Functional Carbon Nanotubes and Graphene Oxide on the Anti-corrosion Performance of Epoxy Coating.” *Polym. Adv. Technol.*, **28** (6) 754–762 (2017)

**Publisher’s Note** Springer Nature remains neutral with regard to jurisdictional claims in published maps and institutional affiliations.